TU Delft

Delft University of Technology

Document Version
Final published version

Licence
CC BY

Citation (APA)
Van Zanten, J. C., Welle, K. T., Ruit, M. V. D., Van Wegen, E. E. H., Meskers, C. G. M., Schouten, A. C., Mugge, W., & Stienen, A. H. A. (2026). Unobtrusive yet Precise Velocity Perturbations During Voluntary Elbow Movement for Reliable Joint Dynamics Assessment. *IEEE Transactions on Neural Systems and Rehabilitation Engineering*, *34*, 1480-1487. https://doi.org/10.1109/TNSRE.2026.3672270

Important note
To cite this publication, please use the final published version (if applicable).
Please check the document version above.

Copyright
In case the licence states “Dutch Copyright Act (Article 25fa)”, this publication was made available Green Open Access via the TU Delft Institutional Repository pursuant to Dutch Copyright Act (Article 25fa, the Taverne amendment). This provision does not affect copyright ownership.
Unless copyright is transferred by contract or statute, it remains with the copyright holder.

Sharing and reuse
Other than for strictly personal use, it is not permitted to download, forward or distribute the text or part of it, without the consent of the author(s) and/or copyright holder(s), unless the work is under an open content license such as Creative Commons.

Takedown policy
Please contact us and provide details if you believe this document breaches copyrights.
We will remove access to the work immediately and investigate your claim.

This work is downloaded from Delft University of Technology.

Unobtrusive Yet Precise Velocity Perturbations During Voluntary Elbow Movement for Reliable Joint Dynamics Assessment

Jonathan C. van Zanten, Karien ter Welle, Mark van de Ruit, Erwin E. H. van Wegen, Carel G. M. Meskers, Alfred C. Schouten, Winfred Mugge, and Arno H. A. Stienen

***Abstract*— Robotic systems assess joint dynamics objectively by perturbing the limb and estimating properties such as impedance. Position perturbations constrain the limb to a target trajectory, reducing variability in task execution but obstructing voluntary motion. Force perturbations allow voluntary movement but elicit orientation-dependent responses, increasing the number of trials needed for accurate estimates. To overcome these limitations, we combined the flexibility of admittance control with the repeatability of position perturbations. A minimum-jerk trajectory ensures smooth transitions. The experiment with six healthy participants was performed to demonstrate the reliability, accuracy and smoothness of applying such perturbations during voluntary movement. Reliability was the proportion of perturbations that reached the target velocity within one millisecond of the acceleration time window. Accuracy was measured as the RMSE between the target and measured velocity during the constant velocity. Smoothness was assessed as perceivability: the fraction of trials in which participants correctly detected a perturbation. The controller allows continuous voluntary movement, switching only during perturbations to impose a precise, specified perturbation. All perturbations reached the target velocity within one millisecond of the acceleration time window; thus, the method is reliable. Under the most demanding condition—an increase to 200 deg/s in 0.01 s—the RMSE between target and measured velocity was 1.1 deg/s (0.55%), indicating a high accuracy. Specially designed perturbations had a perceivability accuracy of 22.1%, indicating smooth transitions between control modes. Together, these results indicate a promising approach for assessing joint dynamics during voluntary elbow movement, enabling assessment during activities of daily living.**

***Index Terms*— Robotic assessment of joint dynamics, voluntary movement, minimum jerk profiles, switching of control modes, velocity/admittance control.**

Received 31 October 2025; revised 9 February 2026; accepted 4 March 2026. Date of publication 9 March 2026; date of current version 19 March 2026. Associate Editor: Helen (He) Huang. *(Corresponding author: Jonathan C. van Zanten.)*

Jonathan C. van Zanten, Karien ter Welle, Mark van de Ruit, Alfred C. Schouten, Winfred Mugge, and Arno H. A. Stienen are with the Department of Biomechanical Engineering, Delft University of Technology, 2628 CD Delft, The Netherlands (e-mail: J.C.vanZanten@tudelft.nl).

Erwin E. H. van Wegen and Carel G. M. Meskers are with Amsterdam University Medical Center, 1081 HV Amsterdam, The Netherlands, and also with Amsterdam Movement Sciences, 1081 HV Amsterdam, The Netherlands.

Digital Object Identifier 10.1109/TNSRE.2026.3672270

I. Introduction

ESTIMATING the joint dynamic properties of the human limbs is essential for understanding neuromuscular control and designing adaptive human–robot interaction frameworks [1], [2], [3], [4]. The joint's dynamic properties, split into the intrinsic and the reflective limb properties, reflect how the human resists perturbations and adapts to different tasks. For assessment of joint dynamic properties for rehabilitation purposes, precise estimates enable safer, more efficient movement and more natural interaction [3].

During static postural tasks, both position and force perturbations can be applied to estimate joint dynamic properties. These perturbations can also be used to separate intrinsic and reflexive limb properties [1], [2], [5], [6], [7]. Under position perturbations, the robot follows the predetermined input position independently of the human response, and joint dynamics estimation is mostly performed in open-loop. With force perturbations, humans can influence the robot's movement, enabling a range of motor control tasks. With force perturbations, estimation of joint dynamics is mostly done in closed-loop [8]. In experiments that require voluntary movement, position perturbations are less practical. The perturbation profile must be generated in advance, which restricts natural, unconstrained behaviour. To overcome this limitation, force perturbations are commonly employed within admittance and impedance control frameworks [9], [10], [11], [12], [13]. However, during voluntary movement, limb orientation and velocity change, and the force-perturbation response depend strongly on them; therefore, many repeated trials are needed for reliable estimates [14]. Other methods of estimating limb dynamics during voluntary movements vary in their methods for assessing joint dynamics, ranging from short-segment analysis [15] to constraining or guiding participants' movements along predefined trajectories, thereby reducing variability and improving estimation robustness [14], [16]. Nevertheless, such constraints may compromise voluntary movement, whereas regular human movements are voluntary and unconstrained. To assess conditions that resemble functional activities, such as activities of daily living (ADLs), joint dynamics should be measured during voluntary movement [17].

We developed a control strategy that combines the flexibility of admittance control with the repeatability of position perturbations, allowing for reliable assessment of joint dynamics during voluntary limb movements. This research improved

© 2026 The Authors. This work is licensed under a Creative Commons Attribution 4.0 License.
For more information, see https://creativecommons.org/licenses/by/4.0/

and extended the control methodology used by Stienen et al. [18], focusing on a smooth switch between control modes. The methodology allows for precisely controlled perturbations during voluntary movement, while offering a high level of flexibility in experiment design. An experiment involving four distinct protocols was conducted to demonstrate the reliability, accuracy and smoothness of applying such perturbations. Reliability was quantified as the proportion of perturbations that reached the target velocity within ± 1 ms of the expected onset of the constant-velocity phase (at the end of the acceleration phase). We used a 1 ms tolerance because early reflex responses occur approximately 20–50 ms after perturbation onset [19]. A 1 ms tolerance corresponds to 5% of the earliest responses within this interval (20 ms).

Accuracy was quantified using the root mean square error (RMSE) between target and measured velocity over the constant-velocity phase. The method was deemed accurate if the RMSE was $< 2\%$ of the target velocity. A tight criterion reduces the risk that unwanted accelerations influence joint-dynamic parameters, as changes in acceleration are known to alter the joint-dynamic parameters [20]. Smoothness was quantified using accuracy of perceivability (AOP), defined as the proportion of correct responses in a perturbation-detection task. Where low perceivability indicates a smooth transition between voluntary movement and controlled perturbation. Perturbations were considered perceivable when performance exceeded the conventional psychophysical threshold (>75% correct), which is commonly used to define discrimination/detection thresholds in proprioceptive assessments [21]. Conversely, performance well below this threshold was taken to indicate a smooth (hard-to-perceive) transition; specifically, we used <25% correct as a conservative 'clearly-below-threshold' criterion.

II. Method

A. Hardware

To analyse the control scheme and the performance of the protocols, we utilised the Shoulder Elbow perturbator (SEP) [22]. The SEP is a diagnostic robotic device which can actively perturb the elbow with adjustable shoulder support. For this experiment, we focused on active elbow function and blocked vertical motion, ensuring only elbow movement. Fig. 1 shows an overview of the SEP, a participant, the movement and an example perturbed velocity profile.

B. Admittance and Velocity Control With Switch

The robotic manipulator employs a control strategy comprising an admittance control loop built according to the guidelines outlined in Keemink et al. [23] to enable voluntary movement, and a velocity control loop to enable precise perturbations. The basis of both controllers is built around the internal velocity servo in the motor driver. The velocity servo has been manually tuned for optimal performance. During velocity control, the input is a target velocity from a perturbation generator, and the controller's output is the measured velocity; the human does not influence the movement. The second mode of control is admittance control. Here, the velocity input to the velocity servo results from the human's applied force, fed through the virtual environment. During admittance control, the human moves the robot within a set virtual environment

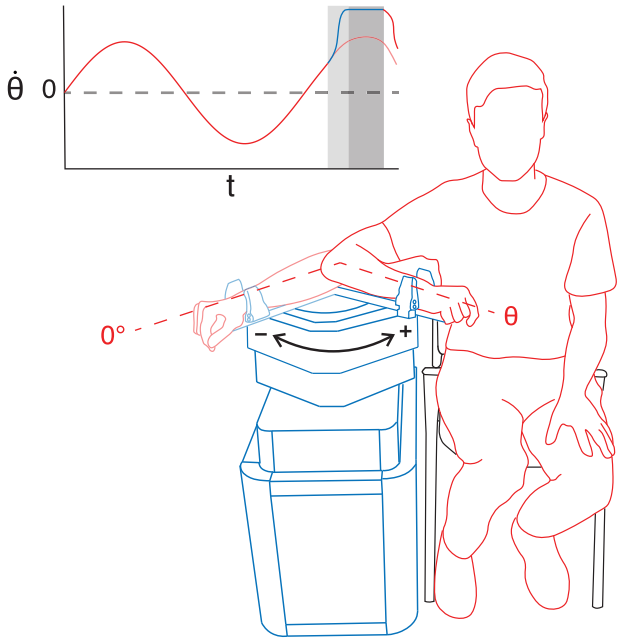

Fig. 1. Illustration of an experimental setup. The elbow's angle (θ) is zero when the arm of a participant is fully extended, and θ represents the current elbow angle. The human is seated and connected to the Shoulder Elbow Pertubator (SEP). The SEP can operate in two modes: velocity control (blue) or admittance control (red). The inset presents the elbow's angular velocity ($\dot{\theta}$) as a function of time when switching between the two control modes throughout voluntary movement. The colours shown in this figure will be assigned to the control modes throughout the paper, unless stated otherwise.

that includes virtual inertia, damping, and stiffness. Fig. 2 provides an overview of the controller, with both control modes and the switch. The switch is placed just before the velocity servo input. It determines whether the velocity servo input comes from the perturbation generator (velocity control) or from the virtual environment (admittance control), enabling switching between the two.

C. Control Switch

A common variable should be used as an input to the internal motor driver to ensure a smooth transition between control modes. For our controller, this is the target velocity. The velocity control mode enables precise perturbations with predefined or instantly generated velocity profiles. Typically, this mode of control is initiated from a set position and begins with the velocity being zero. However, when velocity control is engaged during voluntary movement (following an admittance-to-velocity switch), the initial state at perturbation onset —position, velocity, and acceleration— differs each time. Without perturbation generation based on these values, the difference in velocity and acceleration between the switched control modes results in a noticeable switch. To prevent this, the velocity and acceleration at the moment of the switch are used as inputs to a minimum-jerk profile generator, allowing the system to reach the target velocity within a preset time without sudden changes in acceleration or velocity. At the end of the perturbation, the control mode is switched back to admittance control. The velocity at the instant of the velocity-to-admittance switch is used as the initial condition to prevent a noticeable transition back to admittance control.

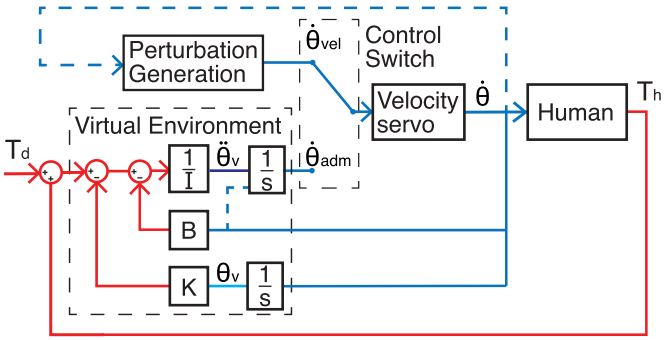

Fig. 2. Control architecture of the Shoulder Elbow Perturbator (SEP) with a switch between admittance (closed-loop) and velocity control (open-loop). In admittance control, human torque T_h drives a virtual environment with stiffness K, damping B, and inertia I; its output is the target acceleration, which is integrated by $1/s$ to the velocity of the virtual environment $\dot{\theta}_{adm}$. This $\dot{\theta}_{adm}$ is tracked by a velocity servo, resulting in the measured velocity $\dot{\theta}$. The Human block comprises the user and the post-sensor device. During velocity control, a perturbation velocity $\dot{\theta}_{vel}$ coming from the minimum jerk perturbation generator is fed directly to the velocity servo, so the human does not influence the motion. The Control Switch selects the active path. A disturbance torque T_d may be applied to the virtual environment, but this study does not consider it. [22]. The dashed blue lines are only used when switching between control modes.

D. Perturbation Generation

During velocity control, the controller may track either a constant target velocity or a time-varying target velocity profile, provided it falls within the elbow's range of motion. To ensure a smooth transition from the current state to the desired velocity, we generate a minimum-jerk transition trajectory [24]. The minimum-jerk generator has the following boundaries and parameters: the initial velocity $v(0)$, initial acceleration $\dot{v}(0)$, the target velocity $v(t_{acc})$, and the allotted transition time t_{acc}.

$$v(0) = \dot{\theta}_{\text{init}}, \qquad \dot{v}(0) = \ddot{\theta}_{\text{init}}, \qquad \ddot{v}(0) = 0, \tag{1}$$

$$v(t_{acc}) = \dot{\theta}_{target}, \qquad \dot{v}(t_{acc}) = 0, \qquad \ddot{v}(t_{acc}) = 0. \tag{2}$$

Equations (1) and (2) specify the boundary conditions of the minimum jerk-profile at $t = 0$ and $t = t_{acc}$.

$$\underbrace{\begin{bmatrix} 1 & 0 & 0 & 0 & 0 & 0 \\ 0 & 1 & 0 & 0 & 0 & 0 \\ 0 & 0 & 2 & 0 & 0 & 0 \\ 1 & T & T^2 & T^3 & T^4 & T^5 \\ 0 & 1 & 2T & 3T^2 & 4T^3 & 5T^4 \\ 0 & 0 & 2 & 6T & 12T^2 & 20T^3 \end{bmatrix}}_{P(T)} \begin{bmatrix} b_0 \\ b_1 \\ b_2 \\ b_3 \\ b_4 \\ b_5 \end{bmatrix} = \underbrace{\begin{bmatrix} \dot{\theta}_{\text{init}} \\ \ddot{\theta}_{\text{init}} \\ 0 \\ \dot{\theta}_{\text{target}} \\ 0 \\ 0 \end{bmatrix}}_{\mathbf{x}} \tag{3}$$

The velocity profile is generated using a fifth-order polynomial in time, where T is the allotted acceleration time ($T = t_{acc}$).

$$\mathbf{b} = P(t_{acc})^{-1}\ \mathbf{x}. \tag{4}$$

Equations (3) and (4) define the corresponding linear system and solve for the coefficient vector $\mathbf{b}$.

$$t_n = \frac{n}{f_s}, \qquad n = 0, 1, \ldots, \lfloor t_{acc} f_s \rfloor - 1, \tag{5}$$

$$v_{\text{acc}}[n] = \sum_{h=0}^{5} b_h\, t_n^h. \tag{6}$$

TABLE I

THIS TABLE GIVES AN OVERVIEW OF THE PERTURBATIONS USED IN THE DIFFERENT PROTOCOLS. v_{target} IS THE TARGET VELOCITY THE ROBOT SHOULD HAVE REACHED A CERTAIN TIME (t_{acc}) AFTER THE PERTURBATION ONSET POSITION (p_{onset}). THE CHANCE IS THE CHANCE THAT A PERTURBATION WILL OCCUR DURING A SINGLE FLEXION AND EXTENSION MOVEMENT

Protocol	Perturbation	v_{target} (deg/s)	t_{acc} (ms)	p_{onset} (deg)	Chance
Long	Slow	100	50	78	1/8
	Fast	200	50	72	1/8
Short	Slow	100	10	88	1/8
	Fast	200	10	82	1/8
Random	Slow	100	50	random	1/8
	Reverse	−100	50	random	1/8
Perception	Slow	100	50	78	1/8
	Fast	200	50	72	1/8
	Long	$v_{\text{init}}+5$	50	78	1/8
	Short	$v_{\text{init}}+5$	10	78	1/8

Finally, the discrete-time velocity profile is obtained by sampling the polynomial at $t_n = n/f_s$, where f_s is the sampling frequency, and n is the integer sample index. Equations (5) and (6) define this sampling and yield the minimum-jerk velocity profile $v_{\text{acc}}[n]$. The index $h = 0, \ldots, 5$ corresponds to the six boundary constraints $\{v(0), \dot{v}(0), \ddot{v}(0), v(t_{acc}), \dot{v}(t_{acc}), \ddot{v}(t_{acc})\}$.

E. Participants

This study included six healthy participants, comprising two females and four males, with two of them having a left dominant hand. All participants were between 25 and 30 years old. Before the experiment, participants were required to read and sign a written informed consent form. The Ethics Committee for Research of Delft University of Technology approved the experimental procedure, with approval number 5775.

F. Experimental Protocol

The experiment consisted of four protocols that offered a variety of conditions to demonstrate that switching between control modes is a reliable, accurate, and smooth way to apply velocity perturbations during voluntary elbow movement. The experiment lasted about 24 minutes and consisted of five four-minute sessions, with one-minute rest in between. The first two sessions used the 'Long' protocol to acquire more data for the analysis; the following sessions used the 'Short', 'Random', and 'Perception' protocols only once to show other possibilities of the methodology. TABLE I shows the perturbations used during these protocols, which consisted of different target velocities and time windows for the minimum-jerk profile, and either set or random onset positions. Since the target velocity and acceleration time in the minimum jerk profiles are changed over the protocols and perturbations, we shift the onset position (p_{onset}) to ensure a constant velocity around 90 degrees across all perturbations. Table I shows the different onset positions. The perception protocol quantified the perceivability of perturbations during voluntary movement to assess switch smoothness and the feasibility

of low-awareness perturbations. Perturbations short and long differed from the other perturbations in the sense that they do not converge to a single velocity but rather add 5 deg/s to the initial velocity. Perturbation short was the only one in the protocol with a 10 ms time window for velocity change, instead of the standard 50 ms.

G. Task

At the start of the experiment, participants were seated with their dominant arm supported and the elbow rotational axis aligned with the robot's axis of rotation. The elbow was fixated to the robotic device by tightening a clamp around the ulnar and radial head of the wrist. They were instructed to perform repeated elbow flexion and extension movements within a comfortable range of motion, which was approximately between 60 and 140 degrees elbow flexion. The movement region was intentionally kept loosely defined to prevent participants from adjusting their movements to remain within this movement region during perturbations. Additionally, participants were instructed to follow a metronome set to 45 beats per minute. At each beat, the participants should have finished either an extension or a flexion. After each extension, the following input was chosen, being either the same perturbation, another perturbation or no perturbation. This selection was done randomly, with the chance of occurrence shown in TABLE I. The input was chosen after extension, as the perturbations only occurred during flexion of the elbow. During the perception protocol, participants held a response button in their non-dominant hand and pressed it whenever they perceived a perturbation; they were instructed not to watch the moving arm.

H. Safety

Our system includes layered hardware and software safety limits. For each participant, the allowable motion range was set to their passive range of motion (pROM) using adjustable mechanical stops. A software 'virtual wall' is implemented 5° before the pROM limit, applying an increasing restoring torque that pushes the joint back toward the safe range. If the joint exceeds the virtual-wall threshold, safety mechanisms are triggered sequentially: (1) a controller end-stop disables commanded motor output, (2) an electrical end-stop removes motor power, and (3) a mechanical end-stop physically prevents further motion in case of equipment malfunction. In addition, both the participant and the operator have access to an emergency stop button that immediately removes power to the motor. Furthermore, the controller allows for individual velocity, acceleration or torque limitations when needed to ensure participant safety.

I. Data Processing

All signals were sampled at $f_s = 2000$ Hz. The same processing was applied to all participants and across all four protocols.

a) Preprocessing: Encoder position p_{raw} was cleaned for obvious spikes: if a single sample changed by more than $v_{\max}/f_s$ with $v_{\max} = 300$ deg/s, that sample was set to NaN and gaps up to 8 ms were linearly interpolated. Position was then smoothed with a zero-phase (forward–backwards) moving average using a 5 ms window; torque was smoothed with a 15 ms moving average. Velocity was computed from the smoothed position using a finite-difference (length-preserving) gradient. Impulsive artefacts were removed with a short Hampel filter (≈ 2 ms, 3 × MAD) to suppress spikes with minimal distortion.

b) Perturbation detection and segmentation: Each perturbation started at the logged mode-of-control switch into the perturbation and ended at the switch back (admittance ↔ velocity; logged as binary). Let s_{ir} and e_{ir} denote the start and end *sample indices* of perturbation trial r for participant i. For each perturbation trial (i, r), we extracted the segment from $t = s_{ir}/f_s - 100$ ms to $t = e_{ir}/f_s + 100$ ms.

c) Tracking error: Within the constant-velocity phase of the perturbation (duration $t_p \leq 100$ ms; shortened if the joint approached its range-of-motion limits), we computed the RMSE between the target velocity and the encoder-derived velocity. Let $n_{s,ir}$ and $n_{e,ir}$ denote the first and last *sample indices* of the constant-velocity phase within perturbation trial (i, r), and let $N_{s,ir}$ denote the number of samples in the constant-velocity window. The constant-velocity phase starts t_{acc} after perturbation onset, so we define

$$n_{s,ir} = s_{ir} + \lfloor t_{\text{acc}} f_s \rfloor, \tag{7}$$

$$n_{e,ir} = \min\Big(n_{s,ir} + \lfloor t_p f_s \rfloor,\ e_{ir}\Big), \tag{8}$$

$$N_{s,ir} = n_{e,ir} - n_{s,ir} + 1. \tag{9}$$

The RMSE over the constant-velocity window is:

$$\text{RMSE}_{ir} = \sqrt{\frac{1}{N_{s,ir}} \sum_{n=n_{s,ir}}^{n_{e,ir}} \Big(v_{\text{tar}}[n] - v_{\text{enc}}[n]\Big)^2}, \tag{10}$$

where $v_{\text{tar}}[n]$ is the target velocity and $v_{\text{enc}}[n]$ is the encoder-derived velocity at sample n.

d) Settling pass rate (SPR): We also report the *Settling Pass Rate* (SPR): the percentage of perturbations whose settling time falls within a specified threshold. First, the settling time of each perturbation trial (i, r) is computed using a 2% band around the target velocity, where k indexes discrete-time samples and $n_{\text{set},ir}$ denotes the earliest sample after which $|v_{\text{enc}} - v_{\text{tar}}|$ remains within the 2% band:

$$\text{band}[k] = 0.02\,\big|v_{\text{tar}}[k]\big|, \tag{11}$$

$$n_{\text{set},ir} = \min\{\, n \in [n_{s,ir}, n_{e,ir}] : \forall k \in [n, n_{e,ir}], \\ |v_{\text{enc}}[k] - v_{\text{tar}}[k]| \leq \text{band}[k] \,\}, \tag{12}$$

$$t_{\text{settle},ir} = \frac{n_{\text{set},ir} - n_{s,ir}}{f_s}. \tag{13}$$

Given a threshold t (e.g., $t = t_{\text{acc}}$, $t = t_{\text{acc}} + 0.5$ ms, or $t = t_{\text{acc}} + 1$ ms), the SPR is:

$$\text{SPR}(t) = 100\,\frac{1}{N_{\text{pert}}} \sum_{i,r} \Big[\, t_{\text{settle},ir} \leq t \,\Big][\%], \tag{14}$$

where N_{pert} is the total number of valid perturbations (valid (i, r) pairs) and $[\cdot]$ is the Iverson bracket (1 if true, 0 otherwise).

e) Coefficient of variation of torque impulse ($CV_p(J_\tau)$): For each participant i and perturbation trial r, we computed the *absolute torque impulse* (units: N m s) over the constant-velocity window $[n_{s,ir}, n_{e,ir}]$. With sampling period $\Delta t = 1/f_s$:

$$J_\tau^{(i,r)} = \sum_{k=n_{s,ir}}^{n_{e,ir}} \big|\tau_i[k]\big|\,\Delta t, \tag{15}$$

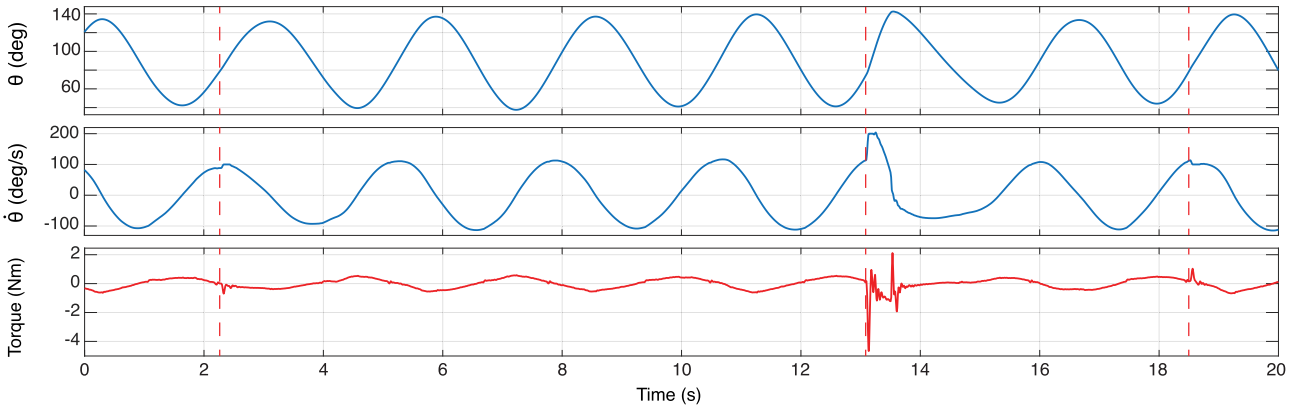

Fig. 3. Typical measurement results of the perturbations for a single participant for the 'Long' protocol. The figure shows one fast (t = 13.1 s) and two slow (t = {2.3, 18.5} s) perturbations; the start of each perturbation is marked with a red dotted line.

where $\tau_i[k]$ denotes the measured torque signal of participant i at sample k.

Within each participant i (for a given protocol/perturbation condition), we calculated the participant mean over n_i valid trials and normalised each trial by that mean:

$$\bar{J}_{\tau,i} = \frac{1}{n_i}\sum_{r=1}^{n_i} J_\tau^{(i,r)}, \qquad R_{ir} = \frac{J_\tau^{(i,r)}}{\bar{J}_{\tau,i}}. \tag{16}$$

We then pooled the within-participant sample variances of R_{ir} (which has mean 1 by definition) to obtain a pooled standard deviation s_p:

$$s_i^2 = \frac{1}{n_i - 1}\sum_{r=1}^{n_i}\left(R_{ir} - 1\right)^2, \qquad s_p = \sqrt{\frac{\sum_i (n_i - 1)\, s_i^2}{\sum_i (n_i - 1)}}. \tag{17}$$

The pooled coefficient of variation is:

$$\mathrm{CV}_p(J_\tau) = 100\, s_p \quad [\%]. \tag{18}$$

The pooled coefficient of variation is a metric showing the consistency of the torque response. When it is low, the torque response across individual trials is close to the mean for that participant and perturbation.

J. Perceptual Analysis

Four perturbations were used in the perception protocol (TABLE I). Because the 'Fast' perturbation has a much higher target velocity, it is likely to be perceived most. To assess the smoothness of the switch, 'Short' and 'Long' perturbations are used. Low percievability is an indication of a smooth switch. For the 'Perception' protocol, we quantified detection performance based on the number of button presses. A *hit* was the first button transition $0 \rightarrow 1$ within a 1 s response window after each perturbation onset. Perturbations which were not followed by a button press were a *miss*. Any click without a perturbation in the last second before the click was a *false hit* (FH).

$$AOP = \frac{\text{hits}}{\text{hits} + \text{misses} + \text{FHs}}. \tag{19}$$

The AOP is determined with equation 19. We report per-participant and total (hits, misses, FHs) counts, as well as AOP. The false hits are also included in the AOP measure, as the human was not perturbed during each movement.

III. Results

Fig. 3 shows the elbow angle, angular velocity and torque of a participant over twenty seconds during the 'Long' protocol. We can see the sinusoidal movement of the elbow. The perturbations are best seen in the velocity window, where multiple perturbations are shown within this particular time frame.

Fig. 4 shows the velocity and torque responses of all participants. The perturbations were averaged, the coloured lines represent the participants' means, and the shaded areas show the participants' standard deviations over the perturbations. The colours represent different participants. The variability in the initial velocity, along with the target velocity, influences the torque response. When examining either the fast or the reverse perturbations, the shaded area around the initial velocity is smaller, indicating greater consistency.

TABLE II shows the accuracy of the velocity perturbations, expressed in RMSE-mean and RMSE-standard deviation for the measured and target velocities during the constant-velocity phase in the perturbation. Overall, the highest RMSE was 1.1 deg/s, which is approximately 0.55% of the corresponding target velocity. The highest percentage was 0.6% of the target velocity, which is lower than the set limit of 2%. TABLE II also shows the SPR(t) for the different perturbation types, with the t being the acceleration time window/ half a millisecond extra/ and a millisecond extra. All perturbations are settled one ms after the desired acceleration time window, with the settling time representing the time it takes for the measured velocity to remain within 2% of the target constant velocity from the start of the perturbation. Lastly, TABLE II shows the coefficient of variation of torque impulse ($\mathrm{CV}_p(J_\tau)$). Low ($\mathrm{CV}_p(J_\tau)$) is an indication of consistency in the torque responses. For perturbations with a larger difference between the initial and target velocities, we observe a much lower CV, indicating greater consistency in the torque response.

A. Perturbation Perception

TABLE III shows the participants' button response to a perturbation. The response can be a hit (perturbation + button click), a miss (perturbation + no button click) and a false hit (FH) (no perturbation + button click). The table also shows the AOP, which was comparable across the different participants. For the perturbations, there was a high but expected

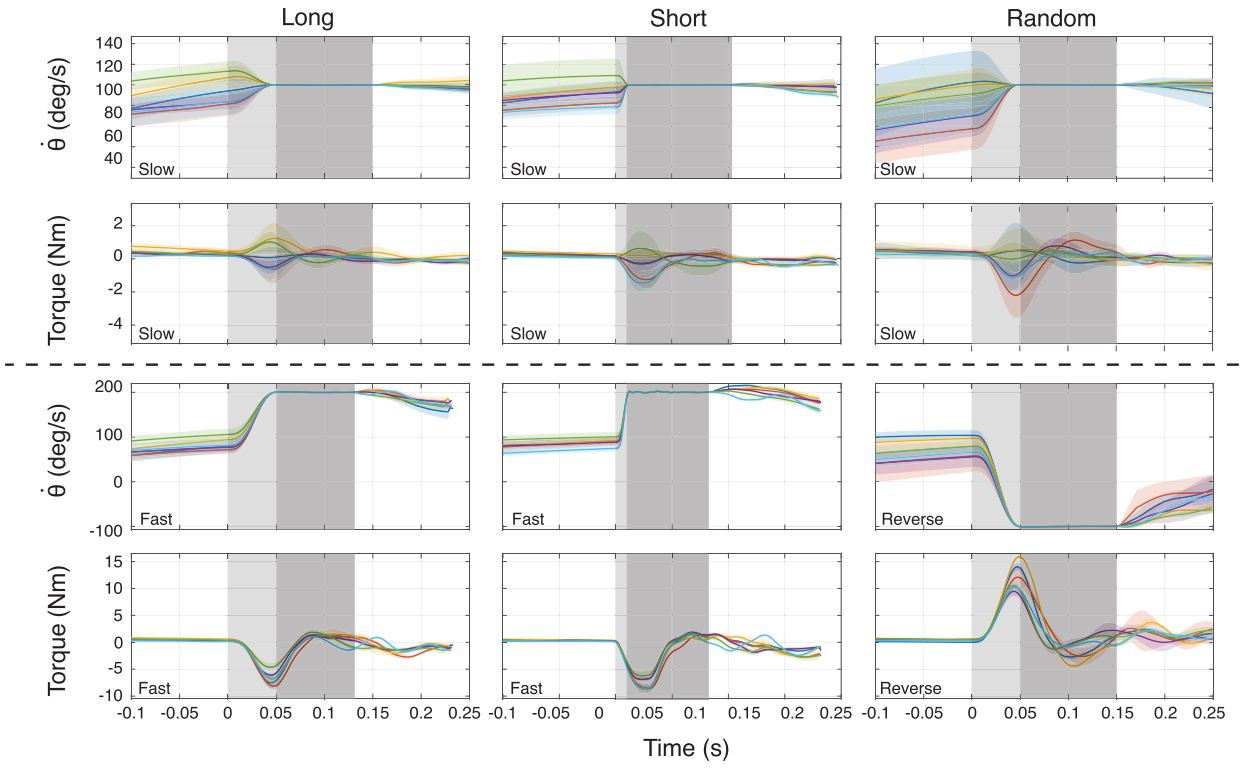

Fig. 4. All participants' velocity and torque response over all perturbations in the 'long', 'short' and 'random' protocols are shown. The perturbations are cut from the signal, with 100 ms of pre- and post-perturbation. The average value during the perturbations is shown with the coloured lines, with different colours representing the participants, and the shaded areas showing the standard deviation. The light grey area represents the minimum-jerk transition, and the dark grey area represents the constant velocity phase.

TABLE II

N_{pert} IS THE NUMBER OF PERTURBATIONS OF A PROTOCOL/ PERTURBATION WITH ALL PARTICIPANTS COMBINED. ROOT MEAN SQUARE ERROR (RMSE), MEAN, AND STANDARD DEVIATION ARE GIVEN PER PROTOCOL/PERTURBATION OVER ALL PARTICIPANTS, TOGETHER WITH THE PERCENTAGE RELATIVE TO THE TARGET. THE SETTLING-TIME PASS RATES (SPR) ARE THE PERCENTAGES OF PERTURBATIONS SETTLED AFTER A CERTAIN TIME, WITH THE TIME BEING THE ACCELERATION TIME WINDOW, HALF A MILLISECOND LATER AND A MILLISECOND LATER. CV MEANS THE POOLED COEFFICIENT OF VARIATION OF THE (ABSOLUTE) TORQUE IMPULSE DURING CONSTANT VELOCITY

	N_{pert} [–]	RMSE mean (std) [deg/s]	RMSE (mean) [% of target]	SPR(t_{acc}/+0.5/+1) ms [%]	$\text{CV}_p(J_\tau)$ [%]
Long — Slow	130	0.1 (0.0)	0.10%	100% / - / -	61.2
Long — Fast	155	0.5 (0.1)	0.25%	100% / - / -	23.6
Short — Slow	56	0.2 (0.1)	0.20%	90.3% / 98.4% / 100%	78.0
Short — Fast	67	1.1 (0.1)	0.55%	0% / 89.0% / 100%	9.1
Random — Slow	56	0.1 (0.1)	0.10%	100% / - / -	70.4
Random — Reverse	54	0.6 (0.1)	0.60%	100% / - / -	22.9

difference in the AOP. The 'Long' and 'Short' perturbations were designed to assess the smoothness of the control mode switch. The 'Long' perturbation had a long time window and a low velocity increase. Here, only 13.2 % of the perturbations were perceived. For perturbation 'Short', the time window decreased, and the AOP increased to 31 %. On average, these specially designed perturbations were only perceived with an AOP of 22.1 %. Perturbations slow and fast were not designed for minimal awareness and were perceived more often with 58.5 % and 98.1 % respectively.

IV. DISCUSSION

The method presented in this paper can be used to apply various velocity perturbations during voluntary movement. The current study implements minimum-jerk velocity perturbations between voluntary movements in admittance control. Across diverse starting states, perturbations reached the target velocity within 1 ms of the acceleration time window, demonstrating reliability. The minimum-jerk generator provides a simple real-time linear ramp. Velocity accuracy was consistent across protocols: RMSE during the constant-velocity phase scaled with perturbation size and window length, but remained $< 0.6\%$, below the 2% accuracy requirement. Overall, the method is reliable and accurate for the tested perturbations.

The acceleration time window of the perturbation, together with the perturbation length, determines the duration of the perturbation. Other studies exploring positional perturbations during voluntary movement mention minimum total

TABLE III
PROTOCOL 'PERCEPTION' - PARTICIPANT REACTION TO VARIOUS PERTURBATIONS SHOWING HITS, MISSES, FALSE HITS AND AOP. ENTRIES MARKED "X" DENOTE NOT APPLICABLE: IN THESE CONDITIONS, A PERTURBATION IS PRESENT BY DEFINITION, SO A FALSE HIT (HIT DETECTED WITHOUT A PERTURBATION) CANNOT OCCUR

Participant/Perturbation	Hits	Misses	False Hits	AOP
P1	28	14	2	0.636
P2	24	14	8	0.522
P3	16	22	0	0.421
P4	10	26	0	0.278
P5	20	28	0	0.417
P6	17	21	0	0.447
Total	**115**	**125**	**10**	**0.454**
Slow	31	21	x	0.585
Fast	51	1	x	0.981
Long	7	45	x	0.132
Short	26	58	x	0.310

perturbation times of 300 ms with acceleration and deceleration times ranging from 100 ms to 120 ms [14] and [16]. Using minimum-jerk perturbations, our method can shorten the total perturbation time. For example, if we assume a similar constant time to that in previous studies —60 ms —and combine it with our short time window for acceleration of 10 ms, the total perturbation time is 70 ms. Reducing the minimum perturbation duration enables additional perturbation designs with shorter time windows that were not feasible with earlier methods. Shorter perturbations also reduce the time available for voluntary responses, which can help isolate the participant's immediate mechanical response.

Consistency in torque responses to perturbations is important for accurate joint dynamics estimation. [17], [25]. A consistent output measure requires a consistent input: if the imposed kinematic perturbation varies across repetitions, the resulting torque response will also vary, inflating variability metrics and degrading parameter estimation. With our methodology, we therefore aim to make the perturbation input as consistent as possible by enforcing a well-defined perturbation profile and evaluating responses over the constant-velocity window. The first measurements with the proposed methodology show high consistency for sufficiently large perturbations (e.g., fast and reverse conditions), with the pooled coefficient of variation remaining below 25% across participants with a limited number of perturbations. While within-participant responses are consistent, torque responses differ across participants, which is expected given inter-individual differences in elbow joint dynamics. Together, the consistent within-participant torque responses and between-participant differences are promising indications that, with appropriate dynamic models, our method can estimate participant-specific joint dynamics using relatively few perturbations.

A. Perturbation Perception

Across the Short and Long perturbations, detection accuracy was 22.1%, indicating accuracy of perception below our criterion determining if transitions are smooth (<25% correct). We therefore interpret these transitions as smooth and compatible with perturbation designs that minimise participant awareness.

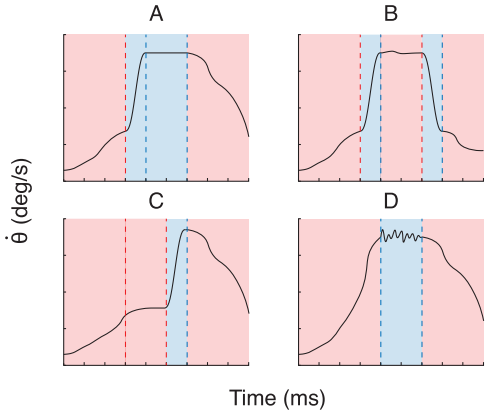

Fig. 5. These are four different possible experiments with the use of the control method described in this paper. Changes in state or parameters are shown with the dashed lines, and the shaded areas represent the admittance control in red and the velocity control in blue. Subfigure A illustrates the current experiment design. Subfigure B shows an example where, after the minimum-jerk profile, the control is switched back to admittance. After a certain period, a reverse minimum-jerk profile is used to return the participant to their original velocity. Subfigure C shows a change in the admittance control. The switch can either be a change in virtual environment parameters or the addition of a disturbance torque. Subfigure D shows a predefined continuous velocity profile, such as a multisine, rather than a ramp-and-hold.

B. Flexibility in Protocol Design

The current experimental protocol demonstrates the method's capability to perform this type of combined control using a switch. Fig. 5 shows four possibilities; by combining the different states, parameters, and switches, a variety of experiments can be conducted using the current methodology. Switches are possible between control modes or within a single control mode by varying parameters. Comparable experiments for the different examples shown in Fig. 5 are done in the following papers. For A, with the use of ramp and hold signals [17], [26], for C with changes in virtual environment [27], [28], and for D with the use of multisine-like signals [15], [29]. Fig. 5 still shows only a limited variety of possible experimental designs. Researchers can utilise the method and design their own experiments, incorporating desired transitions, phases, and parameters as needed for their specific experiments.

C. Limitations and Future Work

This study was performed in a healthy population and therefore does not yet establish applicability in impaired populations. Although multiple software and hardware safety layers were implemented, high-speed perturbations may pose additional considerations in clinical cohorts, including altered joint integrity, spasticity, pain sensitivity, and heightened reflex responses. Future work will therefore focus on clinical implementability by systematically mapping safe and tolerable perturbation parameter ranges (amplitude, peak velocity/acceleration, and timing), quantifying discomfort and task interference, and validating feasibility and utility in relevant patient groups during functional tasks.

A second limitation is that the current validation is limited to a single measured and actuated degree of freedom (DOF) on one hardware platform. Extending the method to multiple DOF introduces coupled dynamics, including configuration-dependent inertia and velocity-dependent Coriolis/centrifugal terms, which increase controller complexity. Consequently,

modelling errors, sensing noise, and delays can propagate across axes, degrading tracking performance and reducing stability margins, particularly at higher speeds and during direction changes. Future work will examine scalability to multi-DOF systems by incorporating cross-coupling into the modelling and control design and by reassessing hardware requirements for accurate, synchronised multi-axis actuation and sensing.

V. Conclusion

This paper introduces and validates a control method that combines precise minimum-jerk velocity perturbations with voluntary elbow movement. Perturbations reached the target velocity within one millisecond of the acceleration time window, regardless of initial state, demonstrating reliability. The low root-mean-square error between the target and actual velocity confirms the accuracy. The decrease in the minimum perturbation time indicates a potential benefit over existing methods. As the transition of control modes is smooth, it enables the design of perturbations which can be delivered with minimal participant awareness, enabling new experiments that probe joint mechanics and motor control without obstructing voluntary movements. Lastly, the consistency in torque response suggests that, with appropriate modelling, participants' joint dynamics can be estimated with relatively few required perturbations. Taken together, these results indicate a promising approach for assessing joint dynamics during voluntary elbow movement, with the potential to support assessment in more functional, daily-life–like contexts.

References

[1] A. C. Schouten, E. de Vlugt, J. J. B. van Hilten, and F. C. T. van der Helm, "Design of a torque-controlled manipulator to analyse the admittance of the wrist joint," *J. Neurosci. Methods*, vol. 154, nos. 1–2, pp. 134–141, Jun. 2006.

[2] F. C. T. van der Helm, A. C. Schouten, E. de Vlugt, and G. G. Brouwn, "Identification of intrinsic and reflexive components of human arm dynamics during postural control," *J. Neurosci. Methods*, vol. 119, no. 1, pp. 1–14, Sep. 2002.

[3] R. E. Kearney and I. Hunter, "System identification of human joint dynamics," *Crit. Rev. Biomed. Eng.*, vol. 18, no. 1, pp. 55–87, 1990.

[4] R. Lundström and L. Burström, "Mechanical impedance of the human hand-arm system," *Int. J. Ind. Ergonom.*, vol. 3, no. 3, pp. 235–242, 1989.

[5] M. van de Ruit et al., "System identification: A feasible, reliable and valid way to quantify upper limb motor impairments," *J. NeuroEngineering Rehabil.*, vol. 20, no. 1, p. 67, May 2023.

[6] W. Mugge, D. A. Abbink, A. C. Schouten, J. P. A. Dewald, and F. C. T. van der Helm, "A rigorous model of reflex function indicates that position and force feedback are flexibly tuned to position and force tasks," *Exp. Brain Res.*, vol. 200, nos. 3–4, pp. 325–340, Jan. 2010.

[7] D. Ludvig, T. S. Visser, H. Giesbrecht, and R. E. Kearney, "Identification of time-varying intrinsic and reflex joint stiffness," *IEEE Trans. Biomed. Eng.*, vol. 58, no. 6, pp. 1715–1723, Jun. 2011.

[8] C. ter Welle et al., "The instrumented assessment of joint neuromechanics in upper motor neuron syndrome—A systematic review," Dept. Biomechanical Eng., Delft Univ. Technol., Delft, The Netherlands, Tech. Rep., 2025.

[9] H. Gomi and M. Kawato, "Human arm stiffness and equilibrium-point trajectory during multi-joint movement," *Biol. Cybern.*, vol. 76, no. 3, pp. 163–171, Apr. 1997.

[10] H. Börner, S. Endo, and S. Hirche, "Estimation of involuntary components of human arm impedance in multi-joint movements via feedback jerk isolation," *Frontiers Neurosci.*, vol. 14, May 2020, Art. no. 459.

[11] M. S. Erden and A. Billard, "Hand impedance measurements during interactive manual welding with a robot," *IEEE Trans. Robot.*, vol. 31, no. 1, pp. 168–179, Feb. 2015.

[12] E. de Vlugt, A. C. Schouten, and F. C. T. van der Helm, "Closed-loop multivariable system identification for the characterization of the dynamic arm compliance using continuous force disturbances: A model study," *J. Neurosci. Methods*, vol. 122, no. 2, pp. 123–140, Jan. 2003.

[13] F. Popescu, J. M. Hidler, and W. Z. Rymer, "Elbow impedance during goal-directed movements," *Exp. Brain Res.*, vol. 152, no. 1, pp. 17–28, Sep. 2003.

[14] E. Burdet, R. Osu, D. W. Franklin, T. Yoshioka, T. E. Milner, and M. Kawato, "A method for measuring endpoint stiffness during multi-joint arm movements," *J. Biomechanics*, vol. 33, no. 12, pp. 1705–1709, Dec. 2000.

[15] D. Ludvig and E. J. Perreault, "Estimation of joint impedance using short data segments," in *Proc. Annu. Int. Conf. IEEE Eng. Med. Biol. Soc.*, Aug. 2011, pp. 4120–4123.

[16] D. J. Bennett, J. M. Hollerbach, Y. Xu, and I. W. Hunter, "Time-varying stiffness of human elbow joint during cyclic voluntary movement," *Exp. Brain Res.*, vol. 88, no. 2, pp. 433–442, Feb. 1992.

[17] D. L. Guarín and R. E. Kearney, "Estimation of time-varying, intrinsic and reflex dynamic joint stiffness during movement. Application to the ankle joint," *Frontiers Comput. Neurosci.*, vol. 11, Jun. 2017, Art. no. 51.

[18] A. H. A. Stienen, J. G. McPherson, A. C. Schouten, and J. P. A. Dewald, "The ACT-4D: A novel rehabilitation robot for the quantification of upper limb motor impairments following brain injury," in *Proc. IEEE Int. Conf. Rehabil. Robot.*, Jun. 2011, pp. 1–6.

[19] V. J. Ravichandran, C. F. Honeycutt, J. Shemmell, and E. J. Perreault, "Instruction-dependent modulation of the long-latency stretch reflex is associated with indicators of startle," *Exp. Brain Res.*, vol. 230, no. 1, pp. 59–69, Sep. 2013.

[20] R. C. van 't Veld, E. H. F. van Asseldonk, H. van der Kooij, and A. C. Schouten, "Disentangling acceleration-, velocity-, and duration-dependency of the short{-} and medium-latency stretch reflexes in the ankle plantarflexors," *J. Neurophysiology*, vol. 126, no. 4, pp. 1015–1029, Oct. 2021.

[21] L. Cappello, N. Elangovan, S. Contu, S. Khosravani, J. Konczak, and L. Masia, "Robot-aided assessment of wrist proprioception," *Frontiers Human Neurosci.*, vol. 9, Apr. 2015.

[22] J. C. van Zanten et al., "System performance analysis of the shoulder elbow perturbator," in *Proc. Int. Conf. Rehabil. Robot. (ICORR)*, May 2025, pp. 346–351.

[23] A. Q. Keemink, H. V. D. Kooij, and A. H. A. Stienen, "Admittance control for physical human–robot interaction," *Int. J. Robot. Res.*, vol. 37, no. 11, pp. 1421–1444, 2018.

[24] K. J. Kyriakopoulos and G. N. Saridis, "Minimum jerk path generation," in *Proc. IEEE Int. Conf. Robot. Autom.*, Apr. 1988, pp. 364–369.

[25] D. A. Kistemaker and L. A. Rozendaal, "In vivo dynamics of the musculoskeletal system cannot be adequately described using a stiffness-damping-inertia model," *PLoS ONE*, vol. 6, no. 5, May 2011, Art. no. e19568.

[26] A. Klomp, J. H. de Groot, E. de Vlugt, C. G. M. Meskers, J. H. Arendzen, and F. C. T. van der Helm, "Perturbation amplitude affects linearly estimated neuromechanical wrist joint properties," *IEEE Trans. Biomed. Eng.*, vol. 61, no. 4, pp. 1005–1014, Apr. 2014.

[27] C. Qi, A. L. Ratschat, M. van de Ruit, and L. Marchal-Crespo, "Effect of modulated robotically rendered viscosity during hand grasping on brain activity," in *Proc. IEEE World Haptics Conf. (WHC)*, Jul. 2025, pp. 228–235.

[28] M. van de Ruit, J. Lataire, F. C. T. van der Helm, W. Mugge, and A. C. Schouten, "Adaptation rate in joint dynamics depends on the time-varying properties of the environment," in *Proc. 7th IEEE Int. Conf. Biomed. Robot. Biomechatronics (Biorob)*, Aug. 2018, pp. 273–278.

[29] M. van de Ruit et al., "Revealing time-varying joint impedance with kernel-based regression and nonparametric decomposition," *IEEE Trans. Control Syst. Technol.*, vol. 28, no. 1, pp. 224–237, Jan. 2020.